



## CHARACTERIZATION OF ALTERED MICA FROM SOKLI, NORTHERN FINLAND

M. RAMA<sup>1</sup>\*, O. EKLUND<sup>1</sup>, S. FRÖJDÖ<sup>1</sup>, J.-H. SMÄTT<sup>2</sup>, M. LASTUSAARI<sup>3</sup>, AND T. LAIHO<sup>4</sup>

<sup>1</sup>Geology and Mineralogy, Faculty of Sciences and Technology, Åbo Akademi University, FI-20500 Turku, Finland

<sup>2</sup>Department of Natural Sciences, Process Chemistry, Åbo Akademi University, FI-20500 Turku, Finland

<sup>3</sup>Centre for Materials and Surfaces, Department of Chemistry, FI-20014 University of Turku, Turku, Finland

<sup>4</sup>Materials Research Laboratory, Department of Physics and Astronomy, FI-20014 University of Turku, Turku, Finland

**Abstract**—Vermiculite is a mineral with many potential uses in various industrial areas, such as in insulation, horticulture, and environmental applications. The regolith of the Sokli carbonatite intrusion in northern Finland consists of weathered micas which reportedly contain vermiculite. The aim of the present study was to characterize the weathered mica in order to determine if the weathered regolith contains vermiculite. If so, the value of the apatite-rich Sokli intrusion may increase, because the vermiculite could be classified as an ore in Sokli. For the characterization, mica fractions were investigated using electron probe microanalysis (EPMA), X-ray diffraction (XRD), and thermogravimetric analysis (TGA). The EPMA results show that the potassium (K<sub>2</sub>O) content of the mica investigated varies between 6.20 and 0.31 wt.%. The XRD results provided evidence that the interlayer distances in the mica vary between 10.1 and 14.7 Å. The TGA shows that the dehydration of the samples varies between 6 and 12 wt.% for temperatures up to 170°C. Dehydroxylation takes place in three steps, as is characteristic for vermiculite. The results from this study revealed that mica in the weathered parts of the Sokli carbonatite is mostly vermiculite, and that the vermiculite was formed by the weathering of phlogopite. These results can be used to determine whether vermiculite is a possible future commodity at the Sokli carbonatite complex.

**Keywords**—EPMA · Phlogopite Alteration · Sokli Carbonatite · TGA · Vermiculite · Vermiculitization · XRD

### INTRODUCTION

The demand for vermiculite has increased recently. The physical and chemical properties of natural vermiculite, such as low density, high cation exchange capacity, and high adsorption ability (Bergaya & Lagaly 2013), are the reasons for using vermiculite in building materials, the chemical industry, and in various applications in environmental protection and agriculture (Huo et al. 2012). Among these uses are as non-flammable packing material, water purification by ion exchange (Rama et al. 2019), and thermal insulation (Bergaya & Lagaly 2013). Exfoliated vermiculite is prepared by heating to >300°C and is used in many commercial applications, such as heat-insulating materials or soil improvers (Suvorov & Skurikhin 2003). Vermiculite is not mined in Finland even though it has been reported to exist at the Sokli carbonatite intrusion (Vartiainen 1974; Kresten & Berggren 1978; O'Brien & Hyvönen 2015).

The Sokli complex is the western-most intrusion of the Kola alkaline province. It is the only part of the province located outside Russia, and is situated 60 km NNW of the Kovdor complex (Krasnova 2001; Lee et al. 2003). Kovdor is known for its rich quarries from which magnetite, apatite, baddeleyite, phlogopite, and vermiculite are excavated. The Sokli massif (and the Kovdor complex) consists principally of an intrusive carbonatite stock with a fenite aureole. In addition to the carbonatites, the massif is composed of ultramafic rocks (dunite and pyroxenite) and multiple stages of phoscorites (forsterite-magnetite-apatite-calcite rocks). Phlogopite is a

common silicate in the Sokli carbonatite (Lee et al. 2003) and vermiculite has reportedly been found both in the carbonatite stock and in the regolith derived from weathering of the phoscorite (Kresten & Berggren 1978). The phoscorite layer in Sokli has a commercial value for the production of phosphorus fertilizers. Vermiculite from the Kovdor regolith has been excavated for commercial use, and Rama et al. (2019) reported a comparison between Sokli and Kovdor vermiculite.

Vermiculite (Mg,Fe,Al)<sub>3</sub>(Al,Si)<sub>4</sub>O<sub>10</sub>(OH)<sub>2</sub>·4(H<sub>2</sub>O) is a mixed-layer phyllosilicate of the hydromica group, and is formed by hydration and other secondary changes of micas, particularly phlogopite (KMg<sub>3</sub>AlSi<sub>3</sub>O<sub>10</sub>(F,OH)<sub>2</sub>) and biotite (K(Mg,Fe)<sub>3</sub>AlSi<sub>3</sub>O<sub>10</sub>(F,OH)<sub>2</sub>) (Ghabru et al. 1989; Deer et al. 1992). According to Roy & Romo (1957) and Komarneni & Roy (1981), vermiculite is a product of mica alteration by dilute, low-alkali solutions. Alternation of different layers along the *c*\* direction can create either ordered or regular mixed-layer structures (Brigatti et al. 2006). Mixed-layer clay minerals with any appreciable degree of randomness show an irregular series of basal reflections in XRD patterns. Mixed-layer biotite-vermiculites are, in most cases, derived from the degradation of pre-existing clay minerals. Previous studies indicated that tri-octahedral biotite could weather to vermiculite under acid conditions, and to vermiculite + montmorillonite under neutral and alkaline conditions (Latimer 1952). The oxidation of Fe(II) to Fe(III) under alkaline conditions causes a large decrease of the clay mineral surface charge and an expansion of the crystal lattice. Based on the analysis of vermiculites and 'hydrobiotites,' Foster (1963) concluded that the composition, charge relation, and cation

\* E-mail address of corresponding author: mrama@abo.fi  
DOI: 10.1007/s42860-019-00041-0

exchange capacity in these vermiculites can be derived from phlogopite or magnesian biotite by the replacement of  $K^+$  by  $Mg^{2+}$ . The term 'hydrobiotite' was interpreted as regular 1:1 interstratification of biotite (or interlayer-deficient biotite) and vermiculite (Rieder et al. 1998; Valášková et al. 2018).

The silicate layers are negatively charged, and electrical neutrality is preserved by the presence of cations between the layers. These interlayer cations are usually  $Mg^{2+}$  or  $Ca^{2+}$ , associated with double layers of water molecules. The interlayer ions are exchangeable and can be replaced by various monovalent or divalent cations (e.g.  $Li^+$ ,  $Na^+$ ,  $K^+$ ,  $Cs^+$ ,  $NH_4^+$ ,  $Ni^{2+}$ ). Pure vermiculite has a cation exchange capacity (CEC) of 1.2–2.4 meq/g (Deer et al. 1992). In addition to the layered structure and large CEC, the third important feature of the vermiculite structure is the variable amount of water in the interlayer space (Tunega & Lischka 2003). The degree of hydration of interlayer cations is a function of the partial vapor pressure of water, the cations, and the charge density in the layers (Whittingham 1989). Due to hydration, the structure of vermiculite can be modified with heat (Kresten & Berggren 1978; Marcos et al. 2009; Mouzadhir et al. 2009).

The occurrence of vermiculite in Sokli has been reported by several authors (Kresten & Berggren 1978; O'Brien & Hyvönen 2015), though there has been no detailed research to confirm the vermiculite findings and the origin of the vermiculite. Prior to commercial utilization, assessment of the quality and estimates of vermiculite reserves are needed. The purpose of the present study was to test the hypothesis that mica flakes from Sokli are mostly vermiculite by performing detailed mineralogical analyses of mica flakes from the weathered surface of the Sokli massif, using a battery of methods, including EPMA, TGA and XRD.

## GEOLOGICAL BACKGROUND AND FIELD RELATIONSHIPS

The Sokli carbonatite complex is located in northeastern Finland, with a center point near 67° 48' 12.2" north latitude and 29° 19' 2.3" east longitude (O'Brien & Hyvönen 2015). The complex was discovered in 1967 in an airborne geophysical survey by the Rautaruukki Company (Paarma 1970). The Sokli carbonatite complex is slightly oval in outline, with a major axis oriented northwest–southeast of ~6.2 km and a minor axis of 4.8 km, covering an area of 20 km<sup>2</sup> (Lee et al. 2003; O'Brien & Hyvönen 2015). Deep seismic sounding data have revealed a conical shape that tapers slightly with increasing depth (Vartiainen 1980). The intrusion consists mainly of calcite carbonatite surrounded by a fenitized aureole (Paarma 1970). The Rb/Sr age of the Sokli carbonatite is 365 ± 3 Ma (Mäkelä & Vartiainen 1978; Kramm et al. 1993). The complex is divided into five geological units (Fig. 1): (1) magmatic core; (2) metasomatic carbonatite surrounding the core; (3) phoscorites and metasomatic phoscorites occurring as large blocks within the carbonatite; (4) transitional zone between the metacarbonatites and fenites; and (5) fenite aureole (Vartiainen 1980; Vartiainen & Vuotovesi 1980; O'Brien et al. 2005).

The magmatic carbonatites of the inner core developed successively in various stages, first by direct crystallization of a carbonatite magma, and later by hydrothermal processes (Vartiainen 1980). The metacarbonatites dominate an area quite clearly outlined against the central core, whereas the contacts with the surrounding transition zone are gradual. The main rock type of the metacarbonatites is metasomatic carbonatite, which was formed by metasomatic replacement of an unidentified lithology by the introduction of CO<sub>2</sub>-rich fluids derived from the carbonatite magma. An arcuate, broken zone of metaphoscorite is located between the metacarbonatite area and the transition zone. The zone was composed initially of ultrabasic rocks comprising magnetite-bearing dunites (partly of pegmatoidal grain size), pyroxenites, and amphibole rocks (Vartiainen 1980). The metaphoscorites are considered as carbonatized alteration products of ultramafites (Vartiainen & Woolley 1976). During multiple metasomatic alteration processes, aegirine, amphiboles, micas, apatite, carbonates, sulfides, and zircons were accommodated in the ultramafites. Within the magmatic core, where metaphoscorites were trapped during the intrusion of the coreplug, the variable effects of magmatic carbonatites complicated still further the development of metaphoscorites (Vartiainen 1980). The transition zone of the metasomatites forms a girdle between the fenite aureole and the metacarbonatite area. The metasomatized zone is composed of fragments of fenites, pyroxenites, hornblendites, mica-amphibole rock, and mica rocks embedded in metasilicosovites (Vartiainen 1980). The fenite aureole is divided into inner syenitic and outer, low-grade fenite areas. The syenitic fenites are completely recrystallized massive rocks with fractures filled by carbonate, aegirine, and sodium amphiboles (Vartiainen & Paarma 1979; Vartiainen 1980).

The Sokli area is covered by weathered bedrock of variable thickness. The most important mineralogical weathering processes are the partial dissolution of carbonates, local replacement of phlogopite by vermiculite, intense alteration of olivine, the partial replacement of magnetite by hematite, alteration of pyrochlore, and the total removal of sulfides (O'Brien & Hyvönen 2015).

The intrusion is capped by a 26-meter-thick regolith that constitutes the main phosphate ore. The phosphorus ore developed from the carbonatite that underwent complex weathering, leaching, recrystallization, and lithification processes (O'Brien & Hyvönen 2015). The P<sub>2</sub>O<sub>5</sub> content in the phosphorus ore ranges from 4 to 5 wt.% to up to 30 wt.%. The consulting and engineering firm Pöyry Environment Oy (2009) estimated the regolith ore reserves to be ~75 Mt by limiting reserves to areas under the thinnest overburden in the Kaulusrova area, where the grade of P<sub>2</sub>O<sub>5</sub> is 5.6 wt.%. In addition to phosphate ore, the deposit contains Nb, Ta, Zr, and some U. According to Vartiainen (1974), the regolith contains up to 10 wt.% mica and the vermiculite content is up to 6 wt.% in the area.

## MATERIALS AND METHODS

### *Sampling and sample preparation*

Soil samples were collected from the regolith altered from carbonatite and phoscorite in the Kaulusrova deposit of the Sokli complex (Sokli9 and Sokli10; Fig. 1). The soil samples

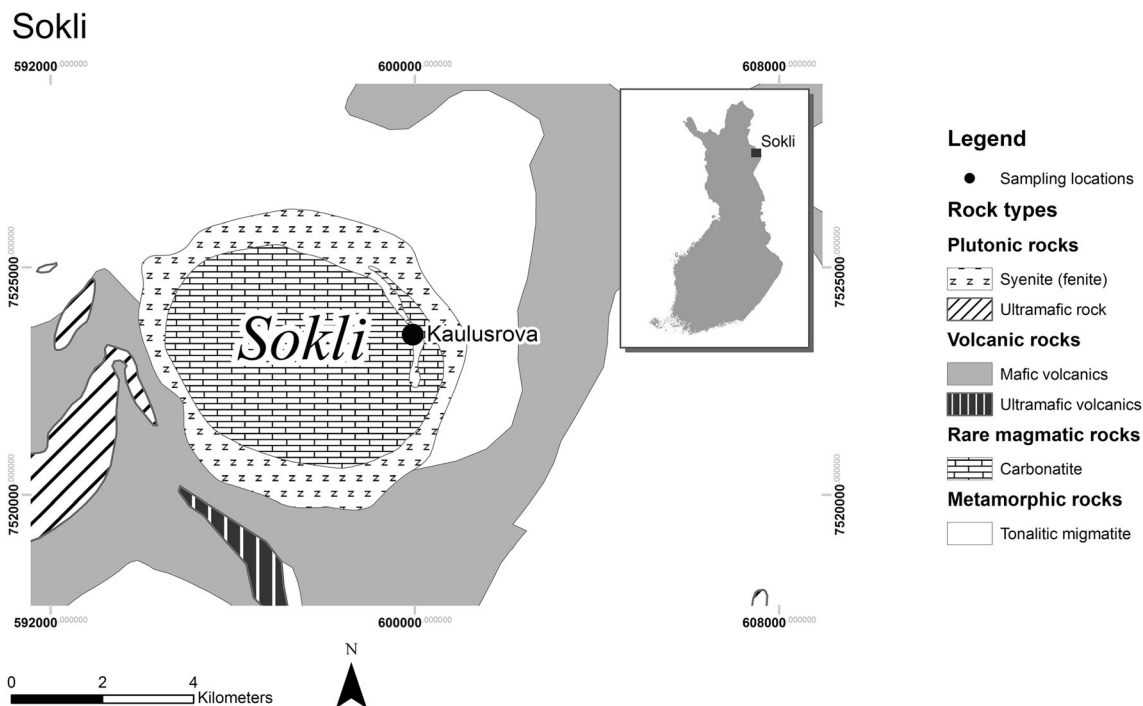


**Figure 1.** Geological map and location of the Sokli complex (Geological Survey of Finland, 2015)

consist mainly of mica and phoscorite, calcite, carbonatite, magnetite, pyroxenites, and amphibole. The soil samples contained ~50% of mica flakes with a grain size varying from ~1 mm to 10 cm. To avoid possible structural damage, the mica flakes were separated from the soil by hand and without any chemical pretreatments or dispersants.

The mica flakes were characterized by EPMA, XRD, and TGA. For XRD and EPMA analyses, mica flakes with a surface size of 11 mm×12 mm and a 3–6 mm thickness from sample Sokli10 were mounted in epoxy and polished (Fig. 2). A Sokli9 sample was used for TGA analysis. This sample was divided into three fractions: a solid sample, Sokli1, with a grain size ~3 cm across and two ground samples, Sokli7 and Sokli8, with a grain size of between 0.075 and 0.125 mm.

#### Analytical methods

The elemental chemical composition of the mica was obtained from wavelength dispersive electron probe microanalysis (WD-EPMA) (JEOL: JXA-8600 superprobe, Tokyo, Japan) at Top Analytica, Turku, Finland, using an accelerating voltage of 15 kV and a beam current of 22 nA. Elemental concentrations were calibrated against natural and synthetic minerals, or pure metals. Data were acquired and ZAF corrections were performed using XMAS software (SMAX 1993).

The XRD measurements were performed using a Bruker D8 Discover (Karlsruhe, Germany) instrument (Laboratory of Physical Chemistry, Åbo Akademi University, Turku, Finland) using a Cu K $\alpha$  X-ray source ( $\lambda = 1.5406 \text{ \AA}$ ) and a scintillation detector. The beam was focused using a 0.5 mm collimator. The various measurement points on the sample were scanned in the range 3–75°2 $\theta$  with an increment of 0.04°2 $\theta$ /0.5 s. The

measurement points were taken for each 1.5 mm on the surface of the sample, and for each 1.0 mm on the cross section.

The thermal response of the mica was studied using a thermogravimetric analyzer (TGA) and differential scanning calorimeter (DSC) - TA Instruments SDT Q600 (New Castle, Delaware, USA) between 25 and 1200°C in flowing air (flow rate: 100 cm<sup>3</sup>min<sup>-1</sup>) (Laboratory of Materials Chemistry and Chemical Analysis, University of Turku, Turku, Finland). Samples of 10 mg each were heated at a rate of 5°C/min. The sample pan

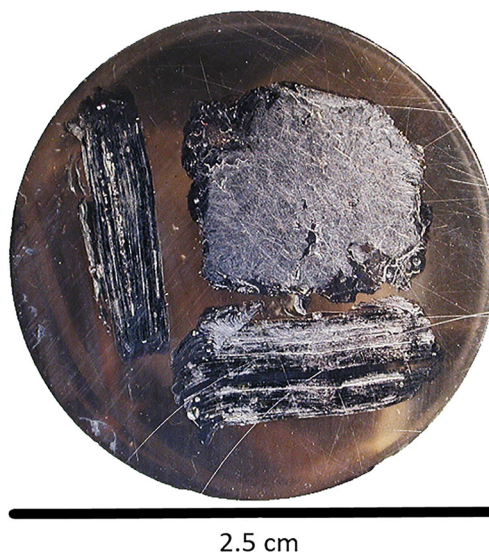


**Figure 2.** Mica flakes (Sokli10) mounted in epoxy exposing either the surface plane (001) or a cross-section of the crystal

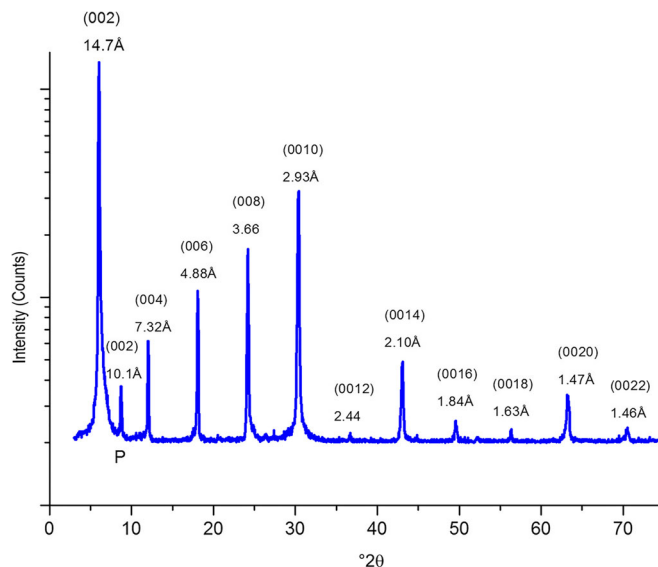


**Figure 3.** XRD pattern of the Sokli10 sample. Crystal plane indices are noted in parentheses and values in Å refer to the spacing. P = phlogopite peak

material was aluminum oxide and an empty aluminum oxide pan was used as a reference. The specific enthalpies of the DSC signals were calculated by integration.

## RESULTS

### XRD results

X-ray diffraction was used to investigate the layer structure and to estimate qualitatively what phases are present in sample Sokli10. The XRD pattern (Fig. 3) clearly displays a main reflection at  $6.04^{\circ}2\theta$ . This strong peak is typical of Mg-vermiculite and can be attributed to the 002 plane, corresponding to an interlayer distance of 14.7 Å (Al-Ani & Saranpää 2008; Barabaszová & Valášková 2013; da Silva et al. 2013). The peak at position  $8.73^{\circ}2\theta$  corresponds to  $d = 10.1$  Å and indicates a small amount of phlogopite ( $\text{KMg}_3\text{AlSi}_3\text{O}_{10}(\text{F},\text{OH})_2$ ), as phlogopite has a basal 002

spacing of 10.0–10.5 Å (Bailey 1980; Chmielarz et al. 2010). Other peaks were detected at  $12.07^{\circ}2\theta$  ( $d = 7.32$  Å),  $18.02^{\circ}2\theta$  ( $d = 4.88$  Å),  $24.21^{\circ}2\theta$  ( $d = 3.66$  Å),  $30.39^{\circ}2\theta$  ( $d = 2.93$  Å),  $43.07^{\circ}2\theta$  ( $d = 2.10$  Å), and  $63.22^{\circ}2\theta$  ( $d = 1.47$  Å). This XRD pattern is characteristic of vermiculite, although  $d$  spacings of vermiculites and other expandable phyllosilicates can vary slightly with changes in relative humidity. Both the intensities and the shapes of the reflections are typical of vermiculite data obtained from the literature (Bailey 1980; Vali & Hesse 1992; Mališ & Křístková 2005; Campos et al. 2009; Hongo et al. 2012; Valášková et al. 2013; Padilla-Ortego et al. 2014). All of the XRD patterns of the vermiculite sample, measured from several points perpendicular to the surface, imply an overall well ordered layered structure. Some small impurities were detected at two positions in the sample. The structure is almost perfectly aligned, as no diffraction peaks could be detected when irradiating the cross-section.

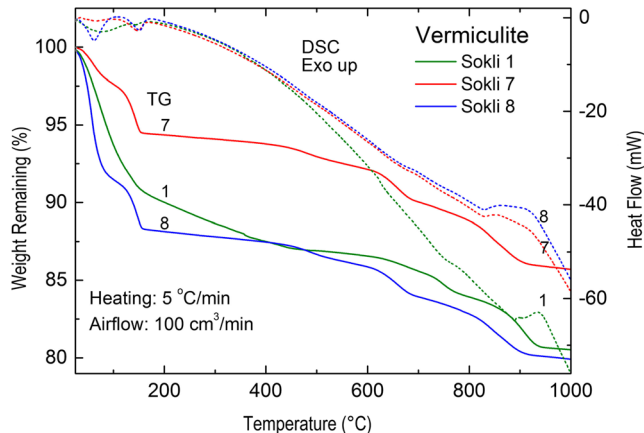


**Figure 4.** Thermogravimetry (TG) and Differential Scanning Calorimetry (DSC) curves for vermiculite from Sokli

**Table 1** Characteristics of dehydration for Sokli vermiculite

Sample	First loss of water (25–75°C)		Second loss of water (75–170°C)		Total Loss (%)
	Loss (%)	$\Delta H$ (Jg <sup>-1</sup> )	Loss (%)	$\Delta H$ (Jg <sup>-1</sup> )	
Sokli1	8	91.3	1	2.7	9
Sokli7	3	19.9	3	65.1	6
Sokli8	9	144.2	3	64.7	12

The XRD patterns of the mica analyzed are clearly similar to those typical of vermiculite with a main reflection 14.7 Å (002). A weak reflection at 10.1 Å (002) indicates interstratification of the mixed-layer structure between phlogopite and vermiculite (Brigatti et al. 2006; Valsásková et al. 2018). Interstratification of phlogopite layers and vermiculite layers are visible in a single grain in Figs 7a and 7b.

#### Temperature dependence results

Thermogravimetry and DSC results are presented to assess the behavior of Sokli vermiculites during dehydration. The temperatures of dehydration reactions of vermiculite vary depending on the relative humidity and the degree of interstratifications with other phyllosilicates, i.e. biotite or phlogopite/vermiculite interstratifications. Due to hydration, the structure of vermiculite can be tailored by thermal treatment.

The dehydration of vermiculite upon heating usually takes place in three steps (Földvári 2011): (1) below and around 100°C, the water adsorbed on the surface is lost; (2) around 200°C, the water between the layers evaporates; and (3) at 250–300°C the water bound to the exchangeable cation escapes.

The TG curves (Fig. 4) show dehydration between room temperature and 200°C only. Two steps of dehydration amounting to 6 wt.% (Sokli7) and 12 wt.% (Sokli8) correspond to loss of the surface water and H<sub>2</sub>O groups between the layers. The first dehydration step differs in magnitude between the two samples, but the second step corresponds to ~3 wt.% for both samples. After this dehydration, the TG curve shows a plateau due to the formation of (Mg,Ca,Fe,Al)<sub>3</sub>((Al,Si)<sub>4</sub>O<sub>10</sub>)(OH)<sub>2</sub>. For the bulk sample (Sokli1), no clear plateau in the TG curve is seen around 200°C, but water constitutes ~9% of the mass. The second loss of water for the bulk sample also shows a very weak signal (Table 1). The dehydration is accompanied by endothermic DSC signals (stippled curves in Fig. 4). The enthalpies involved are shown in Table 1.

**Table 2** Characteristics of dehydroxylation

Sample	First step		Second step		Third step	
	Loss (%)	T (°C)	Loss (%)	T (°C)	Loss (%)	T (°C)
Sokli1	5	155–690	1	690–765	3	765–940
Sokli7	1	420–520	3	520–685	4	685–915
Sokli8	1	410–515	3	515–690	4	690–930

Commonly, the dehydroxylation of vermiculites takes place at 450–850°C (Földvári 2011). For the samples investigated, this process ends at ~950°C. By then, the OH<sup>-</sup> groups have escaped through dehydroxylation from the samples as H<sub>2</sub>O molecules, leaving one O<sup>2-</sup> ion in place of two hydroxide molecules in the vermiculite matrix. This results in the composition (Mg,Ca,Fe,Al)<sub>3</sub>(Al,Si)<sub>4</sub>O<sub>11</sub>. For each sample, the dehydroxylation takes place in three steps (Table 2), but whether these involve endo- or exothermic changes, if any, is difficult to say based on the DSC data. For the ground samples (Sokli7 and Sokli8), the dehydroxylation corresponds to a total mass loss of 8%, whereas the weight loss from the bulk sample was ~9%. The endothermic release of heat at 830°C for samples Sokli7 and Sokli8, and at 895°C for sample Sokli1 (Fig. 4), is a characteristic feature of vermiculite and probably represents the recrystallization to enstatite (Balek et al. 2007; Földvári 2011).

Comparing the mass losses associated with dehydration and dehydroxylation, and assuming an initial composition of (Mg,Ca,Fe,Al)<sub>3</sub>((Al,Si)<sub>4</sub>O<sub>10</sub>)(OH)<sub>2</sub>·nH<sub>2</sub>O, leads to the conclusion that sample Sokli7 is a dihydrate and sample Sokli8 is a trihydrate, whereas sample Sokli1 consists of a mixture of the two. Because sample Sokli1 was not ground, thermal conductivity is lower than that of the ground samples. The dehydration for sample Sokli1 may already have occurred at temperatures up to well above 200°C and the dehydroxylation started before the dehydration was complete, making quantification of the decomposition process more difficult.

X-ray powder diffraction patterns were obtained for all three samples in as-received form as well as after heating for 1 h at 600°C in air. The patterns of the natural vermiculite samples are dominated by the strong (001) reflection at 6°2θ (Fig. 5). The XRD data confirmed that samples Sokli7 and Sokli8 are very similar in composition, which is in agreement with their very similar thermal decomposition. On the other hand, sample Sokli1 is the purest vermiculite of these samples. The XRD data explained why sample Sokli1 behaves clearly differently in the TG measurements.

The XRD patterns recorded after heating the powders for 1 h at 600°C confirmed the expansion of the vermiculite structure, as evidenced by the shift of the reflections to smaller angles (Figs 5 and 6). Also, the loss of some reflections indicated the decomposition of impurities. The expansion is best observed from the shifting of the (001) reflections (Table 3). The dominant (002) reflection of each sample at 5.9°2θ shifted to angles that are smaller than the low-angle

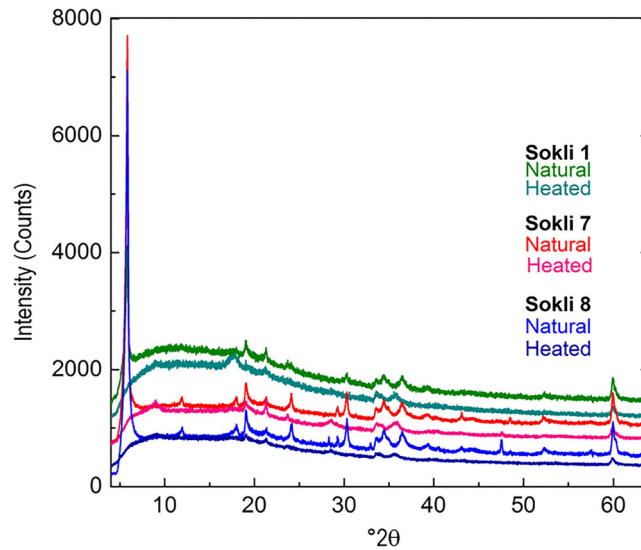


**Figure 5.** Effect of heating on the XRD patterns

limit of the detector ( $4.0^\circ 2\theta$ ), and the expansion had to be studied from the shift in (0010) and (0012) reflections.

#### EPMA results

Back-scattered electron (BSE) images revealed variations in the chemical composition of mica sample Sokli10. Point analyses showed that brighter areas contained more potassium than the darker areas (Fig. 7). The interlayer distance in the sample varied from 10.1 to 14.7 Å, where 10.1 Å was similar to phlogopite and 14.7 Å was similar to Mg-vermiculite (see the XRD results section).

Quantitative chemical analyses were performed on mica sample Sokli10 (Table 1). The amounts of  $\text{SiO}_2$ ,  $\text{Al}_2\text{O}_3$ ,  $\text{MnO}$ , and  $\text{TiO}_2$  were relatively constant.  $\text{MgO}$  and  $\text{Fe}_2\text{O}_3$

composition varied between 25.05 and 17.52 wt.% and 4.17–6.94 wt.%, respectively. The vermiculitization process can be seen in the XRD results as an increase in interlayer space. The areas with the thinnest interlayer have the largest  $\text{K}_2\text{O}$  content, while the layers with the thickest interlayer are depleted in  $\text{K}_2\text{O}$ . Additionally, the areas with the largest  $\text{K}_2\text{O}$  content also have the largest total, while  $\text{K}_2\text{O}$ -depleted micas have the smallest total. The decrease in analytical total may indicate an increase in the non-measured water content in the interlayer of the mica. The decrease in  $\text{K}_2\text{O}$  also represents the vermiculitization process. As  $\text{K}_2\text{O}$  (and  $\text{Na}_2\text{O}$ ) decreases,  $\text{CaO}$  is simultaneously enriched from 0.02 wt.% to 1.88 wt.%. Due to this variation in analyzed points, the vermiculitization process was apparent in this sample.

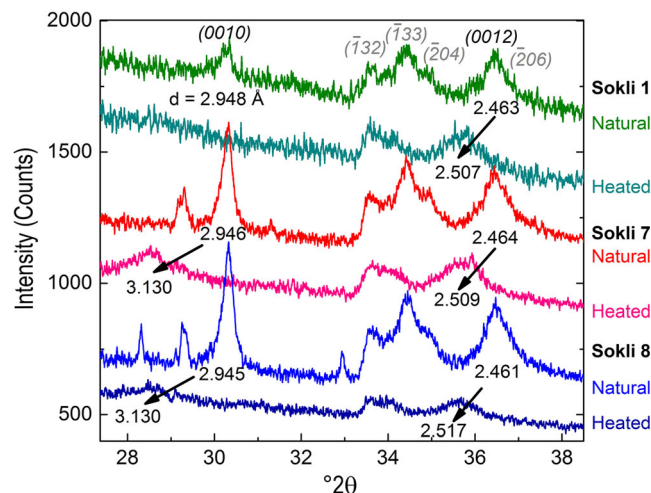


**Figure 6.** Effect of heating on the XRD patterns. The  $hkl$  indices of the reflections belonging to the vermiculite structure are shown. The  $d$  values for the (001) reflections before and after heating are also shown and the shifts are marked with arrows

**Table 3** Effect of heating on the  $d$  values (in Å) of (001) reflections

	(0010)		(0012)	
	Natural	Heated	Natural	Heated
Sokli1	2.948	Too low intensity	2.463	2.507
Sokli7	2.946	3.130	2.464	2.509
Sokli8	2.945	3.130	2.461	2.517

In order to compare the new analyses with literature data, the structural formulae (Table 4) were calculated on the basis of 22 oxygens and assuming all iron to be ferric. The elemental changes in the crystal structure are represented in Fig. 8. Si, Al, and Fe increased progressively, whereas Mg decreased slightly during the vermiculitization at Sokli. These changes are largely similar to those described by Moon et al. (1994).

By using the calculation based on 22 oxygens for the structural formula (Table 4 and Fig. 8), the following trends can be seen: tetrahedral Al decreases with increasing octahedral Al (Fig. 8a), total Al increases with octahedral Al (Fig. 8b), Fe increases with increasing octahedral Al (Fig. 8c), Mg decreases with increasing octahedral Al (Fig. 8d), K decreases with increasing octahedral Al (Fig. 8f), and K decreases with increasing Ca (Fig. 8f).

#### DISCUSSION AND CONCLUSIONS

During the transformation from mica to vermiculite, numerous intermediate mixed-layer phases with various compositions and ordering are formed. As the vermiculite formation process is gradual, lamellae where potassium and ferrous ion concentrations are smaller than

those of phlogopite can exist. Vermiculite differs from micas by not containing  $K^+$  and Fe(II), and having a significant amount of Fe(III) and water. The process of the alteration of mica to vermiculite is conceptualized in the literature as a replacement of  $K^+$  by  $Ca^{2+}$ ,  $Mg^{2+}$ , and  $Al^{3+}$ , oxidation of Fe(II) to Fe(III), and a loss of octahedral cations (Foster 1963; Rieder et al. 1998; Valášková et al. 2018).

An important general feature that illustrates the vermiculitization process is a decrease in K and an increase in water content (Table 4). Another feature is the increase of octahedral Al reported by Moon et al. (1994) and Toksoy-Köksal et al. (2001). The results comply with these characteristics and one can argue that the change from phlogopite to vermiculite occurs in the following way: due to weathering, K is released from the interlayer and Fe is converted from Fe(II) to Fe(III). Removal of K leaves a negative charge which is partly compensated by Ca-bearing fluids from the weathering carbonatite, which bring  $Ca^{2+}$  ions into the interlayer. The octahedral sheet is occupied initially by Fe(II), Mg, and Al, but as the vermiculitization proceeds, Mg is leached out and leaves the system. The negative charge left after loss of Mg is compensated partly by the conversion of Fe(II) to Fe(III). This compensation is insufficient and, consequently, Al is transferred from the tetrahedral sheet to the octahedral sheet and charge balance is partially reached. This sequence is similar to those presented in studies by Nemečz (1981), Banfield & Eggleton (1988), Moore & Reynolds (1989), and Moon et al. (1994).

Calculating the structural formula on the basis of 22 oxygens may not represent the exact distribution of cations in the structural layers, perhaps as a consequence of focusing on cations and ignoring the differing amounts of interlayer water content in the calculations. For example, the absolute  $SiO_2$  content in all analyses appears to be similar (Table 4). If Si is

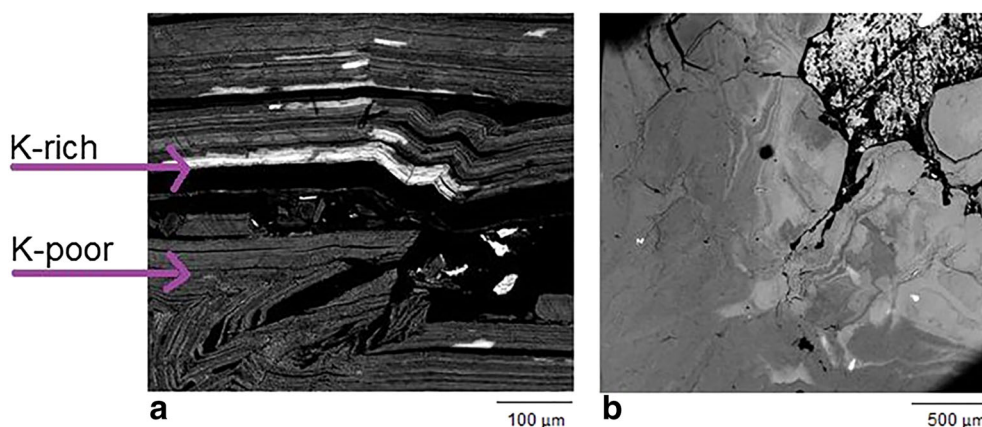


**Figure 7.** Back-scattered electron image of the mica sample Sokli10: (a) cross section and (b) surface. The lighter areas represent greater potassium contents in the mica

**Table 4** EPMA results (wt.%) and structural formula calculated by the method of Deer et al. (1992)

	1 <sup>1</sup>	2	3	4	5	6	7	8	9	10	11	12	13	14
SiO <sub>2</sub>	41.91	41.08	41.42	41.72	40.42	41.94	42.97	41.07	40.48	42.33	41.69	41.76	41.01	41.39
TiO <sub>2</sub>	0.65	0.56	0.64	0.57	0.77	0.53	0.51	0.58	0.61	0.65	0.56	0.47	0.52	0.55
Al <sub>2</sub> O <sub>3</sub>	12.98	14.10	14.21	13.18	13.84	13.53	13.52	13.35	13.54	13.33	13.20	13.36	14.35	13.70
Fe <sub>2</sub> O <sub>3</sub>	4.17	5.54	5.59	5.04	5.16	5.87	5.66	6.94	6.65	6.82	6.40	6.35	6.76	6.41
MnO	0.03	0.02	0.03	0.02	0.06	0.04	0.02	0.05	0.04	0.08	0.04	0.03	0.05	0.05
MgO	25.08	24.38	23.43	20.83	21.01	19.31	19.48	17.52	18.52	18.81	18.09	20.09	19.98	19.07
CaO	0.02	0.03	0.22	0.90	0.45	1.40	1.43	1.30	2.18	1.23	1.29	1.88	1.16	1.42
Na <sub>2</sub> O	0.50	0.79	0.74	0.95	0.74	0.02	0.08	0.03	0.03	0.01	0.01	0.00	0.00	0.02
K <sub>2</sub> O	7.24	6.73	5.93	5.35	4.77	0.28	0.23	0.06	0.05	0.04	0.03	0.02	0.01	0.01
Tot.	88.42	93.86	92.74	87.27	89.77	82.05	82.36	80.90	83.40	82.35	80.62	82.70	85.16	82.91
Number of cations based on 22 oxygen														
Si	5.95	5.85	5.92	6.05	6.18	6.28	6.30	6.36	6.29	6.30	6.36	6.16	6.23	6.30
<sup>IV</sup> Al	2.05	2.15	2.08	1.95	1.82	1.72	1.70	1.64	1.71	1.70	1.64	1.84	1.77	1.70
SUM(IV) <sup>2</sup>	8.00	8.00	8.00	8.00	8.00	8.00	8.00	8.00	8.00	8.00	8.00	8.00	8.00	8.00
<sup>VI</sup> Al	0.12	0.18	0.28	0.37	0.52	0.71	0.72	0.80	0.70	0.69	0.77	0.56	0.72	0.74
Ti	0.07	0.06	0.07	0.06	0.08	0.06	0.06	0.07	0.07	0.07	0.07	0.05	0.06	0.06
Fe <sup>3+</sup>	0.45	0.58	0.59	0.57	0.56	0.67	0.65	0.81	0.75	0.78	0.75	0.73	0.75	0.73
Mn	0.00	0.00	0.00	0.00	0.01	0.01	0.00	0.01	0.00	0.01	0.01	0.00	0.01	0.01
Mg	5.31	5.10	4.93	4.65	4.50	4.40	4.41	4.04	4.16	4.27	4.18	4.56	4.38	4.29
SUM(VI) <sup>3</sup>	5.95	5.92	5.87	5.65	5.68	5.85	5.84	5.72	5.69	5.83	5.78	5.91	5.91	5.82
Mg	0.00	0.00	0.00	0.00	0.00	0.00	0.00	0.00	0.00	0.00	0.00	0.00	0.00	0.00
Ca	0.00	0.00	0.03	0.14	0.07	0.23	0.23	0.22	0.35	0.20	0.21	0.31	0.18	0.23
Na	0.14	0.21	0.20	0.28	0.21	0.01	0.02	0.01	0.01	0.00	0.00	0.00	0.00	0.01
K	1.31	1.20	1.07	1.02	0.87	0.05	0.05	0.01	0.01	0.01	0.01	0.00	0.00	0.00
SUM(i.lyr) <sup>4</sup>	1.45	1.42	1.30	1.44	1.15	0.29	0.30	0.24	0.37	0.21	0.22	0.31	0.19	0.24

<sup>1</sup> Numbers indicate the number of analyzed points

<sup>2</sup> Tetrahedral sheet

<sup>3</sup> Octahedral sheet

<sup>4</sup> Interlayer

fixed in the tetrahedral sites, Si should be constant, and Al should fill the rest of the available vacancies in the tetrahedra. The Al that does not fit the tetrahedral sites is situated in the octahedral sites. Fluctuation of the water content (and other fluids) and the form of water (H<sub>2</sub>O or OH<sup>-</sup>) may produce negatively charged vacancies in the lattice that can be occupied by cations that do not fit a theoretical filling of the structure based on 22 oxygens. The sum of octahedral cations does not exceed 6 in any of the points measured, which is likely due to the leached-out Mg.

This study adds information identifying vermiculite as a possible future commodity at the Sokli carbonatite complex and may improve the economic value of the Sokli intrusion by identifying the vermiculite at Sokli as a valuable resource. Mica clay from the regolith overlying the Sokli complex in northeastern Finland was

characterized using EPMA, XRD, and TG-DSC techniques. Vermiculite is the dominant mica mineral in the deposit. The combined results indicate that the investigated phases correspond to vermiculite, with subordinate amounts of phlogopite. The presence of phlogopite is indicated by varying K<sub>2</sub>O contents (0.0–8.0 wt.%) and by XRD diffractograms showing a pattern typical of natural Mg-vermiculite. The TG and DSC results showed different thermal behavior in the samples investigated because of differences in chemical composition. The dehydration of Sokli vermiculite took place in two steps over the temperature range 25–170°C. The dehydration-induced diminution of interlayer distance typical of vermiculite was observed clearly in the XRD patterns measured before and after the heating of samples for 1 h at 600°C.



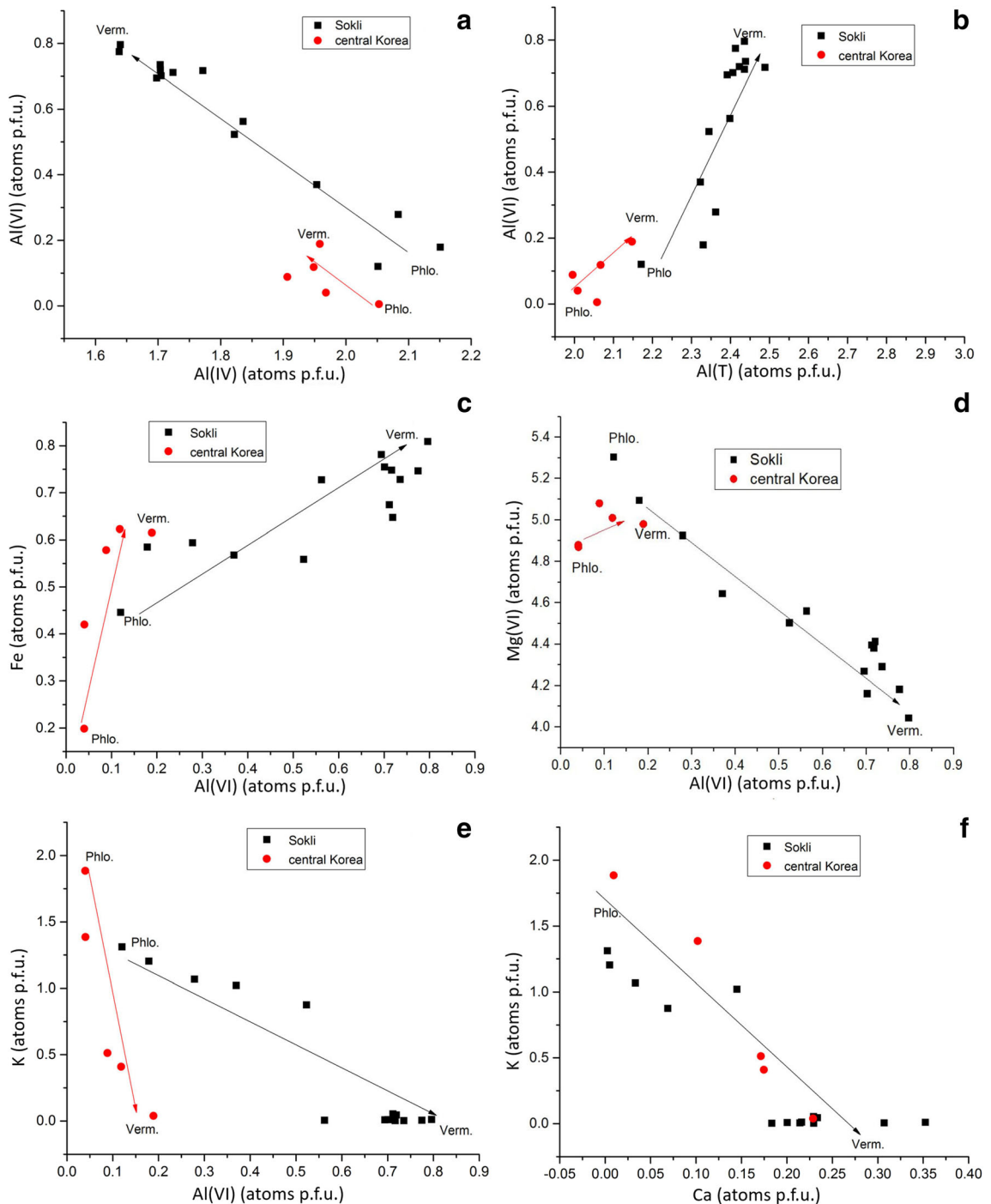


**Figure 8.** Compositional variation of atoms per formula unit (atoms p.f.u.) diagrams for investigated mica from Sokli (black squares) compared with analyses from Moon et al. (2008) (red dots): (a)  $^{IV}Al$  vs.  $^{VI}Al$ ; (b)  $Al(tot)$  vs.  $^{VI}Al$ ; (c)  $Fe(tot)$  vs.  $^{VI}Al$ ; (d)  $Mg$  vs.  $Mg(tot)$ ; (e)  $K$  vs.  $^{VI}Al$ ; and (f)  $K$  vs.  $Ca$ . In the graphics,  $^{IV}Al$  is tetrahedral aluminum,  $^{VI}Al$  is octahedral aluminum,  $Al(tot)$  is total aluminum, and  $^{VI}Mg$  is octahedral magnesium

## ACKNOWLEDGMENTS

Open access funding was provided by the Abo Akademi University (ABO). This paper is a part of the PhD study by the first author (M.R.) at the Faculty of Science and Engineering, Geology and Mineralogy at Åbo Akademi University. The first author is grateful to the Finnish Doctoral Program in Geology and K.H. Renlund's foundation for supporting this study.

**Open Access** This article is distributed under the terms of the Creative Commons Attribution 4.0 International License (<http://creativecommons.org/licenses/by/4.0/>), which permits unrestricted use, distribution, and reproduction in any medium, provided you give appropriate credit to the original author(s) and the source, provide a link to the Creative Commons license, and indicate if changes were made.

## REFERENCES

- Al-Ani, T., & Sarapää, O. (2008). *Clay and clay mineralogy, physical-chemical properties and industrial uses*. Geological Survey of Finland report M19/3232/2008/41.
- Balek, V., Pérez-Rodríguez, J. L., Pérez-Maqueda, L. A., Šubrt, J., & Poyato, J. (2007). Thermal behaviour of ground vermiculite. *Journal of Thermal Analysis and Calorimetry*, 88, 819–823.
- Banfield, J. E., & Eggleton, R. A. (1988). Transmission electron microscope study of biotite weathering. *Clays and Clay Minerals*, 36, 382–403.
- Barabaszová, K. Č., & Valášková, M. (2013). Characterization of vermiculite particles after different milling techniques. *Powder Technology*, 239, 277–283.
- Bergaya, F., & Lagaly, G. (2013). General Introduction: Clays, Clay Minerals, and Clay Science. Pp 1–17 in: *Handbook of Clay Science, 2nd Edition* (F. Bergaya and G. Lagaly, editors). Volume 5A, Elsevier, Amsterdam.
- Brigatti, M. F., Galán, E., & Theng, B. K. G. (2006). Structures and mineralogy of clay minerals. In F. Bergaya, B. K. G. Theng, & G. Lagaly (Eds.), *Handbook of Clay Science, 1st Edition* (pp. 19–86). Amsterdam: Elsevier.
- Bailey, S.W. (1980) Structure of Layer Silicates. Pp. 2–124 in: *Crystal Structures of Clay Minerals and their X-Ray Identification* (G.W. Brindley and G. Brown, editors). Monograph 5, Mineralogical Society, London.
- Campos, A., Moreno, S., & Molina, R. (2009). Characterization of vermiculite by XRD and spectroscopic techniques. *Earth Sciences Research Journal*, 13, 108–118.
- Chmielarz, L., Kowalczyk, A., Michalik, M., Dudek, B., Piwowska, Z., & Matusiewicz, A. (2010). Acid-activated vermiculites and phlogopites as catalysts for the DeNOx process. *Applied Clay Science*, 49, 156–162.
- Da Silva, A. A. S., Sampaio, J. A., da Luz, A. B., Franca, S. C. A., & Roconi, C. M. (2013). Modelling controlled potassium release from phlogopite in solution: Exploring the viability of using crushed phlogopite rock as an alternative potassium source in Brazilian soil. *Journal of the Brazilian Chemical Society*, 24, 1366–1372.
- Deer, W. A., Howie, R. A., & Zussman, J. (1992). *An Introduction to the Rock Forming Minerals* (2nd ed.). London: Longman.
- Foster, M. D. (1963). Interpretation of the composition of vermiculites and hydrobiotites. *Clays and Clay Minerals*, 70–89.
- Földvári, M. (2011). *Handbook of thermogravimetric system of minerals and its use in geological practice*. Budapest: Occasional papers of the Geological Institute of Hungary.
- Geological Survey of Finland (2015). Bedrock map 1:100 000. [http://hakku.gtk.fi/locations/search?location\\_id=11](http://hakku.gtk.fi/locations/search?location_id=11). Accessed 27 October 2015.
- Ghabru, S. K., Mermut, A. R., & Arnaud, R. J. (1989). Layer-charge and cation-exchange characteristics of vermiculite (weathered biotite) isolated from a gray luvisol in northeastern Saskatchewan. *Clays and Clay Minerals*, 37, 164–172.
- Hongo, T., Yoshino, S., Ymazaki, A., Ymazaki, A., & Sarokawa, S. (2012). Mechanochemical treatment of vermiculite in vibration milling and its effect on lead (II) adsorption ability. *Applied Clay Science*, 70, 77–78.
- Huo, X., Wu, L., Liao, L., Xia, Z., & Wang, L. (2012). The effect of interlayer cations on the expansion of vermiculite. *Powder Technology*, 224, 241–246.
- Komameni, S., & Roy, R. (1981). Hydrothermal transformations in candidate overpack materials and their effects on Cesium and strontium sorption. *Nuclear Technology*, 54, 118–122.
- Kramm, U., Kogarko, L. N., Kononova, V. A., & Vartiainen, H. (1993). The Kola Alkaline Province of the CIS and Finland: Precise Rb-Sr ages define 380–360 Ma age range for all magmatism. *Lithos*, 30, 33–44.
- Krasnova, N. (2001). The Kovdor phlogopite deposit, Kola Peninsula, Russia. *The Canadian Mineralogist*, 39, 33–44.
- Kresten, P., & Berggren, G. (1978). The thermal decomposition of vermiculite. *Thermochimica Acta*, 23, 171–182.
- Latimer, W. M. (1952). *Oxidation Potential* (2nd ed.). New York: Prentice-Hall.
- Lee, M. J., Garcia, D., Moutte, J., & Lee, J. I. (2003). Phlogopite and tetraferriphlogopite from phoscorite and carbonatite associations in the Sokli massif, Northern Finland. *Geosciences Journal*, 7, 9–20.
- Mališ, J., & Křístková, M. (2005). Structure of vermiculite modified by organic molecules. *Acta Geodynamica et Geomaterialia*, 2, 105–111.
- Marcos, C., Arango, Y. C., & Rodriguez, I. (2009). X-ray diffraction studies of the thermal behaviour of commercial vermiculites. *Applied Clay Science*, 42, 368–378.
- Moon, H.-S., Song, Y., & Lee, S. Y. (1994). Supergene vermiculitization of phlogopite and biotite in ultramafic and mafic rocks, Central Korea. *Clays and Clay Minerals*, 42, 259–268.
- Moore, D. M., & Reynolds, R. C. (1989). *X-ray Diffraction and the Identification and Analysis of Clay Minerals* (2nd ed.). Oxford: Oxford University Press.
- Mouzdahir, Y. E., Elmchauri, A., Mahboub, R., Gil, A., & Korili, S. A. (2009). Synthesis of nano-layered vermiculite of low density by thermal treatment. *Powder Technology*, 189, 2–5.
- Mäkelä, M., & Vartiainen, H. (1978). A study of sulfur isotopes in the Sokli multisatage carbonatite (Finland). *Chemical Geology*, 21, 257–265.
- Nemecz, E. (1981). *Clay Minerals*. Budapest: Akademiai Kiado.
- O'Brien, H.E., Peltonen P., & Vartiainen, H. (2005). Kimberlites, carbonatites and alkaline rocks. Pp. 605–644 in: *Precambrian Geology of Finland – Key to the evolution of the Fennoscandian shield* (M. Lehtinen, P.A. Nurmi, and O.T. Rämö (editors). Elsevier.
- O'Brien, H. E. and Hyvönen, E. (2015). The Sokli carbonatite complex. Pp. 305–325 in: *Mineral deposits of Finland* (W.D. Maier, R. Lahtinen, and H. O'Brien, editors). Elsevier.
- Paarma, H. (1970). A new find of carbonatite in North Finland, the Sokli plug in Savukoski. *Lithos*, 3, 129–133.
- Padilla-Ortego, E., Leyva-Ramos, R., & Mendoza-Barron, J. (2014). Role of electrostatic interactions in the adsorption of cadmium (II) from aqueous solution onto vermiculite. *Applied Clay Science*, 88–89, 10–17.
- Pöyry Environment Oy (2009). Sokli mine environmental impact statement, p.86. <http://www.ymparisto.fi/download/noname/%7B9FF4A1D4-C572-4C7A-865D-143DD32F0B33%7D/42576>. Accessed 28 February 2019.
- Rama, M., Laiho, T., Eklund, O., & Wärmå, J. (2019). An evaluation of the capability of nanomodified vermiculite to in situ ammonium removal from landfill leachate. *Environmental Technology & Innovation*, 10, 100340.
- Rieder, M., Cavazzini, G., Dyakonov, Y. S., Frank-Kamenetskii, V. A., Gottardi, G., Guggenheim, S., Koval, P. V., Müller, G., Neiva, A. M. R., Radoslovich, E. W., Robert, J. L., Sassi, F. P., Takeda, H., Weiss, Z., & Wones, D. R. (1998). Nomenclature of the micas. *The Canadian Mineralogist*, 36, 905–912.
- Roy, R., & Romo, L. A. (1957). Weathering studies: New data on vermiculite. *Geology Journal*, 65, 603–610.

- Suvorov, S. A., & Skurikhin, V. V. (2003). Vermiculite — a promising material for high-temperature heat insulators. *Refractories and Industrial Ceramics*, 3, 186–193.
- Toksoy-Köksal, F., Türkmenglu, A. G., & Göncüoğlu, M. C. (2001). Vermiculitization of phlogopite in metagabbro, central Turkey. *Clays and Clay Minerals*, 49, 81–91.
- Tunega, D., & Lischka, H. (2003). Effect of the Si/Al ordering on structural parameters and the energetic stabilization of vermiculites – a theoretical study. *Physics and Chemistry of Minerals*, 30, 517–522.
- Vali, H., & Hesse, R. (1992). Identification of vermiculite by transmission electron microscopy and X-ray diffraction. *Clay Minerals*, 27, 185–192.
- Valášková, M., Tokarský, J., Hundáková, M., Zdrálková, J., & Smetana, B. (2013). Role of vermiculite and zirconium-vermiculite on the formation of zircon-cordierite nanocomposites. *Applied Clay Science*, 75–76, 100–108.
- Valášková, M., Kupková, J., Martynková, G. S., Seidlerová, J., Tomášek, V., Ritz, M., Kočí, K., Klemm, V., & Rafaja, D. (2018). Comparable study of vermiculites from four commercial deposits prepared with fixed ceria nanoparticles. *Applied Clay Science*, 151, 164–174.
- Vartiainen, H. (1974). Kaulusrovan ojatutkimus, RO4/75.
- Vartiainen, H. (1980). The petrography, mineralogy and petrochemistry of the Sokli carbonatite massif, northern Finland. *Geological Survey of Finland Bulletin*, 313, 126 pp.
- Vartiainen, H., & Vuotovesi, T. (1980). The Sokli carbonatite complex. *Lithos*, 13, 224–225.
- Vartiainen, H., & Paarma, H. (1979). Geological characteristics of the Sokli carbonatite complex, Finland. *Economic Geology*, 74, 1296–1306.
- Vartiainen, H., & Woolley, R. (1976). The petrography, mineralogy and chemistry of the fenites of the Sokli carbonatite intrusion. *Geological survey of Finland Bulletin*, 280, 87 pp.
- Whittingham, M. S. (1989). Transport properties of the mineral vermiculite. *Solid State Ionics*, 32(33), 344–349.
- SAMx Products (1993). XMAS software for the microanalysis. Trappes, France.